Tellus
SERIES A
DYNAMIC
METEOROLOGY
AND OCEANOGRAPHY
PUBLISHED BY THE INTERNATIONAL METEOROLOGICAL INSTITUTE IN STOCKHOLM

Tellus (2010), 62A, 10–23

Spatio-temporal evolution of perturbations in ensembles initialized by bred, Lyapunov and singular vectors

By DIEGO PAZÓ*, MIGUEL A. RODRÍGUEZ and JUAN M. LÓPEZ, *Instituto de Física de Cantabria (IFCA), CSIC–UC, Avenida de Los Castros, 39005 Santander, Spain*

(Manuscript received 12 June 2009; in final form 12 October 2009)

ABSTRACT

We study the evolution of finite perturbations in the Lorenz '96 model, a meteorological toy model of the atmosphere. The initial perturbations are chosen to be aligned along different dynamic vectors: bred, Lyapunov, and singular vectors. Using a particular vector determines not only the amplification rate of the perturbation but also the spatial structure of the perturbation and its stability under the evolution of the flow. The evolution of perturbations is systematically studied by means of the so-called mean-variance of logarithms diagram that provides in a very compact way the basic information to analyse the spatial structure. We discuss the corresponding advantages of using those different vectors for preparing initial perturbations to be used in ensemble prediction systems, focusing on key properties: dynamic adaptation to the flow, robustness, equivalence between members of the ensemble, etc. Among all the vectors considered here, the so-called characteristic Lyapunov vectors are possibly optimal, in the sense that they are both perfectly adapted to the flow and extremely robust.

1. Introduction

Making predictions in systems with spatio-temporal chaos involves not only an analysis of error amplifications, coming from model uncertainties and assimilation defects, but also a study of the spatial propagation of perturbations. Apart from the interest of being a fundamental study of chaotic dynamics, suited perturbations are daily used in weather forecasting in the generation of initial ensembles (Kalnay, 2002). The so-called Ensemble Prediction System (EPS), which is the main operative tool used in today's forecasting, estimates the error evolution by means of deterministic forecast integration given by a model (Tracton and Kalnay, 1993; Molteni et al., 1996). Differences between these forecasts (members of the ensemble) are finite perturbations. The choice of a proper initial ensemble is crucial for the final result and some kind of control—in order to obtain a determined statistics or spread on the initial ensemble evolution—is necessary. The deterministic character of a chaotic system should provide this possibility, but up to now this choice is based on more or less phenomenological arguments, leading to controversies about the use of bred versus singular vectors (SVs) (Errico and Langland, 1999; Toth et al., 1999). The main obstacle is the complexity of weather models that impedes a precise treatment in the generation of perturbations (Wei and Frederiksen, 2004). The simple characterization of perturbations can be difficult due to the existence of several temporal scales and characteristic lengths (Primo et al., 2007). Even in the case of simplified models, a complete picture of the potential use of finite or infinitesimal perturbations as initial ensembles is actually lacking. Most of the existing studies limit their analysis to the behaviour of the perturbation amplitude (the norm), paying very little or no attention to the differences in the spatial structure of bred, Lyapunov or SVs (Smith, 2001).

In a system with chaos in space and time the norm of an infinitesimal random perturbation always grows exponentially, but the collapse to the main Lyapunov vector (involving spatial propagation of errors) evolves slowly with a power law in time (López et al., 2004). Since space and time play complementary roles it is easy to find scaling laws relating both variables. These laws are important because they can completely determine the main features of a perturbation in both their generation and their evolution. In the past few years, it has been shown that a very convenient way to study these processes is through a logarithmic transformation of the perturbation (Pikovsky and Kurths, 1994; Pikovsky and Politi, 1998; López et al., 2004; Primo et al., 2005, 2006; Szendro et al., 2007; Pazó et al., 2008, 2009). Indeed, many properties are not only generic but universal in quantitative terms for a broad family of spatio-temporal chaotic systems.

*Corresponding author.
e-mail: pazo@ifca.unican.es
DOI: 10.1111/j.1600-0870.2009.00419.x

For the sake of simplicity we restrict our analysis to errors due to initial perturbations, hence we are assuming the hypothesis of perfect model. Perturbations of this kind can be simulated taking a 'control' trajectory of the system $\mathbf{y}(t)$ and integrating in parallel another copy of the system $\mathbf{y}'(t)$ obtained by perturbing the control trajectory at $t = 0$: $\mathbf{y}'(0) = \mathbf{y}(0) + \mathbf{v}(0)$. In our study, the perturbation $\mathbf{v}$ is applied along either a bred, Lyapunov, or SV. In this paper we characterize the spatio-temporal dynamics of the perturbation as time evolves, $\mathbf{v}(t) = \mathbf{y}'(t) - \mathbf{y}(t)$.

An ensemble of perturbations for probabilistic forecasting purposes can be constructed from a given set of initial perturbations $\mathbf{v}$ by using different methods (Kalnay, 2002) but the choice of the members of that ensemble (the perturbation vectors $\mathbf{v}$ or a suitable combination of them) is of a major relevance for the final result. Two major approaches are currently used in operative weather forecasting based on EPSs to try to efficiently sample the uncertainty related to the initial condition assessment by introducing appropriate initial perturbations. On the one hand, there are ensembles of bred vectors, which are finite perturbations that are grown from the past trajectory of the models. On the other hand, there are operative forecasting techniques that mostly use SVs, which capture the directions of maximal growth in a fixed time window in the future. Although much work has been devoted to the development of techniques for the generation of such ensembles, still little is known about the spatiotemporal evolution of the initial perturbations themselves (i.e. the members of the ensemble) and their spatio-temporal correlations. Understanding the spatio-temporal behaviour of the members of the ensemble (either bred, singular or others) is a fundamental, still open, question that needs to be solved to be able to construct ensembles of perturbations that serve better for the purpose.

In preparing an ensemble of initial perturbations there is a number of properties that are desirable. The four most outstanding properties usually required are the following: (i) Dynamic adaptation: initial perturbations should be well embedded in the attractor, this can be achieved by growing perturbations from the (remote) past. (ii) Reliability and equivalence among the members of the ensemble: One wants the perturbations to be statistically equivalent but at the same time to have enough diversity to capture a significant portion of the phase space. (iii) Analysis of error: the ensemble should be able to capture differences between the analysis and the true atmospheric state. Finally, (iv) fastest spread: The ensemble should be able to sample the fastest growth directions in phase space, so that the more unstable directions are well represented. To obtain an ensemble that performs well with one or two of these requirements is relatively easy, but producing ensembles with members that satisfy all these properties is a tremendously difficult problem, which in our opinion is still unresolved. In order to improve our design of ensembles it is fundamental to understand better the spatio-temporal properties of the perturbation vectors to be used.

The aim of this paper is to explore the possibilities of control on the evolution of the ensemble using bred, singular, and Lyapunov vectors in a simple model of spatial chaos. Obviously, by controlling the ensemble evolution a more adapted probabilistic forecast can be performed, which confers practical interest to our study. On one hand, we have the basic elements to address this study on a firm theoretical basis, by characterizing the elements (initial vectors) with physical properties such as correlation lengths and crossover times, and their generation and evolution by space–time scaling properties (Primo et al., 2005). On the other hand, there exists a very simple representation of the dynamics of perturbations, the recently introduced mean-variance of the logarithm (MVL) diagram (Primo et al., 2005, 2007; Gutiérrez et al., 2008), which provides in a condensed form information about their state. This diagram is a very general representation of a chaotic evolution in which temporal and structural evolutions are graphically represented in a sort of simple phase space.

The paper is organized as follows. Section 2 is devoted to introduce the model and its associated linear operator to propagate infinitesimal perturbations. In Section 3, the definition and fundamental properties of the dynamic vectors used are briefly presented. Sections 4–6 deal with the main aspects in the description of the perturbation growth, the norm, the spatial localization and the spatial structure. Section 7 is a brief introduction to the MVL diagram as a tool to represent the evolution of finite perturbations. Section 8 deals with the evolution of free finite perturbations initialized by bred, Lyapunov, and SVs. Taking these results in mind, Section 9 includes a short digression about the use of different (dynamic) vectors to prepare initial ensembles. Finally, some conclusions about the use of dynamic vectors to control some aspects in the evolution of an ensemble of initial perturbations are outlined in the conclusions (Section 10).

2. Lorenz '96 model

In order to gain intuition about the evolution of ensembles of different types of perturbations we restrict ourselves in this paper to a model that is simple enough to allow us fast simulations with good statistics, while at the same time the model displays complex behaviour and spatio-temporal chaos. Our numerical simulations were carried out in the equation proposed by Lorenz (1996) as a toy model of weather dynamics. We consider a one-dimensional array of variables $\mathbf{y}(t) = \{y_x(t)\}_{x=1,\ldots,L}$ with periodic boundary conditions

$$\frac{\mathrm{d}}{\mathrm{d}t} y_x = -y_x - y_{x-1}(y_{x-2} - y_{x+1}) + F. \tag{1}$$

The variables y_x may be looked at as the values of some unspecified scalar meteorological observable, like a vorticity or temperature, at equally spaced sites extending around a latitude circle (Lorenz and Emanuel, 1998). The L96 model (1)

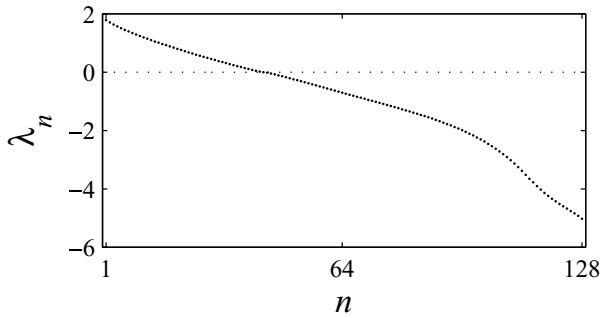

Fig. 1. Lyapunov spectrum of the Lorenz '96 model for $F = 8$ and a system size $L = 128$. Lyapunov exponents are disposed following the standard ordering ($\lambda_n \geq \lambda_{n+1}$). ($\lambda_1 \cong 1.78$ and $\lambda_{43} = 0$.)

contains quadratic, linear and constant terms mimicking advection, dissipation and external forcing, respectively. We take $F = 8$ and typically use $L = 128$ throughout the paper. This leads to a highly chaotic dynamics as demonstrated by the Lyapunov exponents shown in Fig. 1 . The Lyapunov spectrum has been computed by means of the well-known algorithm of Benettin et al. (1980) using the tangent space evolution equation

$$\frac{\mathrm{d}}{\mathrm{d}t}\delta y_x = -\delta y_x - \delta y_{x-1}(y_{x-2} - y_{x+1}) - y_{x-1}(\delta y_{x-2} - \delta y_{x+1}). \tag{2}$$

A linear operator $\mathbf{A}$ allows one to obtain the perturbation at time t from the perturbation at an earlier time t_0

$$\delta\mathbf{y}(t) = \mathbf{A}(t, t_0)\delta\mathbf{y}(t_0). \tag{3}$$

In contrast with infinitesimal perturbations, the evolution of a finite perturbation $\mathbf{v}\,(t)$ is computed explicitly from the difference between the two distinct trajectories initiated from slightly different initial conditions: $v(x, t) = y_x'(t) - y_x(t)$.

3. Fundamentals: bred, Lyapunov and singular vectors

Perturbation dynamics in extended chaotic systems can be analysed by using different types of vectors. These vectors are generically called 'Lyapunov vectors', however, they are actually different quantities by construction and they indeed contain different type of information about the chaotic trajectory depending on its magnitude (infinitesimal or finite), the temporal interval for the calculation (finite or quasi-infinite; past, future or both). Next we briefly introduce the vectors we will be considering in this paper, and recall their most outstanding properties, which are summarized in Table 1. The use of these vectors is widespread in the specialized literature because they provide a fundamental tool to characterize space–time chaos in different contexts ranging from theoretical studies to actual weather forecasting with operative models.

3.1. Backward Lyapunov vectors (B-LVs)

Following Legras and Vautard (1996), we distinguish backward, forward and characteristic Lyapunov vectors (LVs). Backward Lyapunov vectors (B-LVs) are the vectors obtained integrating eq. (2) by means of the Gram–Schmidt orthogonalization procedure. They appear, for instance, as a byproduct of the popular algorithm of Benettin et al. (1980) to obtain the Lyapunov exponents (LEs). There exists a B-LV $\mathbf{b}_n$ for each Lyapunov exponent λ_n. At $t = 0$ the B-LV corresponding to the largest LE, $\mathbf{b}_1(t = 0)$, is called the first (or main) LV and gives the orientation at present time, $t = 0$, of a perturbation after integrating eq. (3) from a random infinitesimal initial perturbation in the remote past (formally from $t_0 = -\infty$). B-LVs corresponding to other LEs must be orthogonalized to avoid the collapse along the direction of the first vector. This makes B-LVs for $n > 1$ to be dependent of the specific scalar product used. It was rigorously proven by Ershov and Potapov (1998) that B-LVs obtained in the Benettin method are indeed eigenvectors of $\mathbf{A}\mathbf{A}^*$. Throughout this paper we adopt the standard scalar product in the Euclidean space and thus $\mathbf{A}^* = \mathbf{A}^{\mathrm{T}}$.

Backward LVs have information from the past but not from the future. Accordingly, LEs are recovered only when integrating these vectors backwards: $\lim_{t\to-\infty} t^{-1} \ln ||\mathbf{A}(t, 0)\, \mathbf{b}_n(0)|| = \lambda_n$. In contrast, forward integration results in a growth with the generic exponential rate λ_1 for all of them. It is important to

Table 1. Different vectors and properties

Vector type	Notation	Magnitude	Computation interval	Eigenvector of	Control parameter(s)
Log-BV	$\mathbf{l}_{M_0}$	Finite	$(-\infty, 0)$	—	M_0
B-LV	$\mathbf{b}_n$	Infinitesimal	$(-\infty, 0)$	$\mathbf{A}(0, -\infty)\, \mathbf{A}^*(0, -\infty)$	n ($\leftrightarrow n$-th LE)
F-LV	$\mathbf{f}_n$	Infinitesimal	$(0, \infty)$	$\mathbf{A}^*(\infty, 0)\, \mathbf{A}(\infty, 0)$	n ($\leftrightarrow n$-th LE)
C-LV	$\mathbf{g}_n$	Infinitesimal	$(-\infty, 0) \cup (0, \infty)$	—	n ($\leftrightarrow n$-th LE)
SV	$\mathbf{s}_\tau$	Infinitesimal	$(0, \tau)$	$\mathbf{A}^*(\tau, 0)\, \mathbf{A}(\tau, 0)$	τ (here $n = 1$ only)

Notes: The computation time indicates which temporal range is needed to obtain each vector at time $t = 0$; in practice infinite-time limits are replaced by sufficiently long times. Notation: Log-BV, logarithmic bred vector; B-LV, backward Lyapunov vector; F-LV, forward Lyapunov vector; C-LV, characteristic Lyapunov vector; SV, forward singular vector. For SVs, only the eigenvector with the largest eigenvalue ($n = 1$) is considered.

stress that, due to the constraint of orthogonality, the B-LVs are not covariant with the dynamics: $\mathbf{b}_n(t > 0) \neq \mathbf{A}\,(t, 0)\,\mathbf{b}_n(0)$, for $n > 1$. Nonetheless, they are well adapted to the flow (B-LVs corresponding to positive LEs point inside the attractor) because they are perturbations that have evolved from the remote past, capturing the convergence of volumes in phase space towards the strange attractor via the stretching-and-folding mechanism.

3.2. Forward Lyapunov vectors (F-LVs)

Forward LVs (F-LVs) are the time-reversed counterpart of B-LVs. F-LVs are generated as B-LVs but integrating backwards from the far future. Therefore, F-LVs are not well adapted to the dynamics (they are not tangent to the attractor), but in contrast with B-LVs, the corresponding λ_n are recovered when integrating these vectors forwards $\lim_{t\to\infty} t^{-1} \ln ||\mathbf{A}(t, 0)\,\mathbf{f}_n(0)|| = \lambda_n$. Backward integration, however, results in a exponential growth with the same rate $-\lambda_L$ for all of them. So, again F-LVs are not covariant with the dynamics.

3.3. Characteristic Lyapunov vectors (C-LVs)

Characteristic Lyapunov vectors (C-LVs) were discussed thirty years ago by Ruelle (1979), however, their numerically calculation in extended systems had remained a difficult problem from a computational point of view. C-LVs are independent of the definition of the scalar product, and in addition, they are covariant with the (forward and backward) dynamics

$$\mathbf{g}_n(t) = \mathbf{A}(t, 0)\mathbf{g}_n(0), \tag{4}$$

for either $t > 0$ or $t < 0$. As a consequence, the associated expansion rate is recovered in both, the future and past limits

$$\lim_{|t|\to\infty} t^{-1} \ln ||\mathbf{A}(t, 0)\mathbf{g}_n(0)|| = \lambda_n. \tag{5}$$

This guarantees that C-LVs are well adapted to the flow (like B-LVs) while expanding with the corresponding LE (like F-LVs). In fact B-LVs and F-LVs in their backward and forward evolution tend, respectively, to their corresponding C-LV before being affected by computing errors.

Among all vectors used in this work C-LVs are the only ones that are computed using information from both past and future. For $n = 1$ the C-LV is simply $\mathbf{g}_1 \propto \mathbf{b}_1$. However, the computation of the C-LVs for $n > 1$ is much more involved. They are obtained by intersecting in a proper manner the spaces spanned by backward and forward Lyapunov vectors (Eckmann and Ruelle, 1985; Legras and Vautard, 1996). To compute C-LVs we have used the algorithm recently introduced by Wolfe and Samelson (2007) and we refer the interested reader to that paper to obtain further details about the calculation.

3.4. Singular vectors

The forward SV is the disturbance that yields the largest linear growth over a specified future time interval τ. Similarly, there exists a backward SV defined as the disturbance that has grown the most after some time interval. However, backward SVs are of lesser importance, at least in the context of weather forecasting, and will not be considered here. Thus we will simply refer to forward SVs as singular vectors. Other vectors generated in finite time intervals, like the so-called finite-time normal modes (Wei and Frederiksen, 2004), exhibit essentially the same asymptotic statistical structure (cf. fig. 2 in Pazó et al., 2009). As occurs for the Lyapunov vectors one can construct a full spectrum of SVs as the set of eigenvectors of $\mathbf{A}^*(\tau, 0)\,\mathbf{A}(\tau, 0)$, which are again dependent of the norm chosen. However, we will only study here the SV with the largest eigenvalue (i.e. the most expanding one) and focus on the influence of the optimization time τ. Note that when the optimization time diverges the SV aligns with the F-LV, $\lim_{\tau\to\infty} \mathbf{s}_\tau \propto \mathbf{f}_1$, obeying universal scaling laws (Pazó et al., 2009).

3.5. Logarithmic bred vectors (Log-BVs)

Bred vectors are *finite* perturbations generated (or 'bred') by imposing that the perturbed system $\mathbf{y}'(t)$ stays within some fixed finite distance from the control trajectory $\mathbf{y}(t)$ (Kalnay, 2002). In practice this is simply achieved by rescaling the error to a given size ϵ_0 every few time steps. Given a prefixed time interval T the difference between control and perturbed trajectories $\mathbf{l}(t_m) = \mathbf{y}'(t_m) - \mathbf{y}(t_m)$ is computed at times $t_m = mT$. At each iteration of the rescaling procedure, the 'perturbed system' is redefined as $\mathbf{y}'(t_m) = \mathbf{y}(t_m) + \epsilon_0\mathbf{l}(t_m)/||\mathbf{l}(t_m)||$, and allowed evolve freely until the next rescaling is scheduled at time t_{m+1}. The (finite) error $\mathbf{l}\,(t)$ constructed in this way is the so-called bred vector at time t. The time interval T has to be chosen small enough to maintain perturbation integrity, apart from that, T is arbitrary and only sets the unit of time used. Here we use $T = 1$ t.u. (time units) without loss of generality.

An important aspect of breeding, although not fully recognized in the literature, is the choice of the norm. As was showed by Primo et al. (2005), and to be argued in detail below, the geometric or zero-norm $||\mathbf{l}(t)||_0 \equiv \prod_{x=1}^{L} |l(x, t)|^{1/L}$ (see below) turns out to be the most convenient in the case of spatio-temporal chaotic systems. The use of the zero-norm leads to the so-called 'logarithmic' bred vectors (Log-BVs), as a type of bred vectors for which it is possible to control the spatial structure (Primo et al., 2005, 2006, 2008). We have found convenient to parameterize the Log-BVs by the logarithm of its magnitude, thus we define $M_0 = \ln \epsilon_0$. Note that for very small magnitudes the bred vector becomes a quasi-infinitesimal perturbation and, therefore, it becomes approximately collinear with the first Lyapunov vector. In other words: $\lim_{M_0\to-\infty} \mathbf{l}_{M_0} \propto \mathbf{b}_1$. Therefore, since bred vectors are finite perturbations, the size of the Log-BV

determines whether we are in the linear (or non-linear) evolution regime.

4. Error growth

Our numerical experiments in this paper are carried out as follows. We take an initial condition $\mathbf{y}(0)$ that corresponds to a state of the system after a sufficiently long transient. Then, we consider a slightly perturbed state $\mathbf{y}'(0) = \mathbf{y}(0) + \mathbf{v}(0)$, where $\mathbf{v}(0)$ is a finite small perturbation proportional to one of the dynamic vectors presented in the preceding section: $\mathbf{v} \propto \{\mathbf{b}_n, \mathbf{f}_n, \mathbf{g}_n, \mathbf{s}_\tau, \mathbf{l}_{M_0}\}$. Then, we let both control and perturbed systems to evolve freely and monitor the dynamics of the perturbation $\mathbf{v}(t) = \mathbf{y}(t) - \mathbf{y}'(t)$ in time. Let us stress here that all perturbations studied in this paper are truly finite errors of the control trajectory, $\mathbf{y}(t)$, initialized along the directions of different types of infinitesimal (B-LV, F-LV, C-LV and SV) or finite size (L-BV) vectors. Therefore, their time evolution is governed by the full non-linear equation and saturation is expected when the error size approaches the attractor size.

In this section, we look at the free evolution of different finite perturbations by focusing on their most apparent property—namely, the average growth in time. This already poses some questions concerning the norm to be used in this analysis.

Among all q-norms of a vector $\mathbf{v}$

$$||\mathbf{v}(t)||_q \equiv \left[\frac{1}{L}\sum_{x=1}^{L}|v(x,t)|^q\right]^{1/q} \tag{6}$$

the 0-norm (or geometric norm)

$$||\mathbf{v}(t)||_0 \equiv \lim_{q\to 0}||\mathbf{v}(t)||_q = \prod_{x=1}^{L}|v(x,t)|^{1/L} \tag{7}$$

is known to be the least fluctuating one for computing the Lyapunov spectrum (Pikovsky and Politi, 1998). This property actually derives from the multiplicative character of infinitesimal error growth and its intrinsic log-normal statistics (Primo et al., 2005).

As error growth in chaotic systems is generically exponential, it is convenient to work with the logarithm of the 0-norm. So, we define

$$M(t) = \langle \ln ||\mathbf{v}||_0\rangle = \left\langle \frac{1}{L}\sum_{x=1}^{L}\ln|v(x,t)|\right\rangle = \left\langle \frac{1}{L}\sum_{x=1}^{L}h(x,t)\right\rangle, \tag{8}$$

where $h(x,t) \equiv \ln|v(x,t)|$ is an auxiliary field whose significance will be clear below, and the angular brackets indicate averages over independent initial conditions.

Figure 2 shows $M(t)$ for perturbations initialized by a representative set of different vectors, all of them started in the quasi-infinitesimal regime $M(0) = -16$. In all cases the perturbation saturates when it reaches the typical size of the attractor

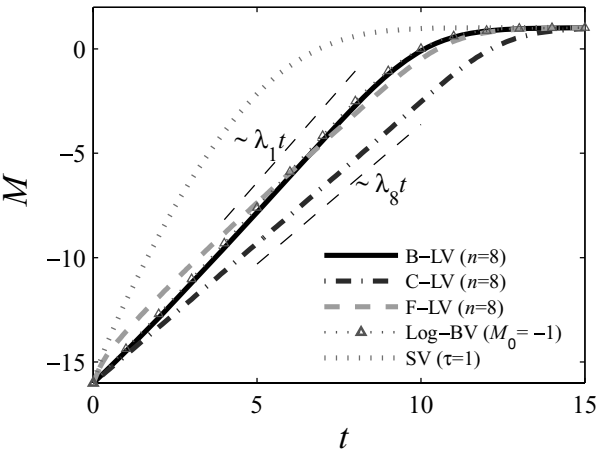

Fig. 2. Evolution of $M(t)$ for initial perturbations along a representative set of vector types. In all cases the initial perturbation was set to have $M(t=0) = -16$. $M(t)$ was averaged over 5000 realizations. Note that all vectors saturate when $M(t)$ reaches a certain size because they are finite perturbations (see Section 4).

$M \approx 1$. In the linear regime ($M \ll 0$) different behaviours are observed depending on the initial perturbation type and in full agreement with the theory. The SV is optimized to grow the most in a time interval and the perturbation initialized along it clearly overcomes all the other vector types. For the Log-BV and the 8th backward LV $M(t)$ almost overlap sharing the same growth rate λ_1. The 8th characteristic LV however yields a growth rate that nicely fits with the eighth LE λ_8, as expected. Although, for sake of clarity, only the 8th vector is shown, the same occurs for any characteristic vector (2nd, 3rd and so on) corresponding to an expanding direction ($\lambda_n > 0$).

The behaviour using the nth forward LV merits some discussion. $\mathbf{f}_n$ is contained within the subspace spanned by characteristic vectors $\{\mathbf{g}_n, \ldots, \mathbf{g}_L\}$. Therefore, the linear evolution in the long time limit will be dominated by the most expanding C-LV $\mathbf{g}_n$. In Fig. 2, the vectors have a finite time (∼10 t.u.) before non-linear effects become important. However the contribution of the subdominant characteristic LV $\mathbf{g}_9$ becomes negligible only after a transient larger than $(\lambda_8 - \lambda_9)^{-1} \approx 19.4$ t.u. Due to these limitations we can only observe that after an initial fast growth, the slope becomes smaller than λ_1(λ_8 is the theoretical limit in the absence of non-linearities and numerical round-off errors). Again, a similar caveat has to be considered when using the 2nd, 3rd, ... forward LVs.

5. Surface width and localization

Any useful theoretical description of perturbation growth in spatially extended chaotic systems must explain how an initially random perturbation acquires structure in space over the course of time through the interaction of the very many spatial degrees of freedom. This is ultimately related with the manner

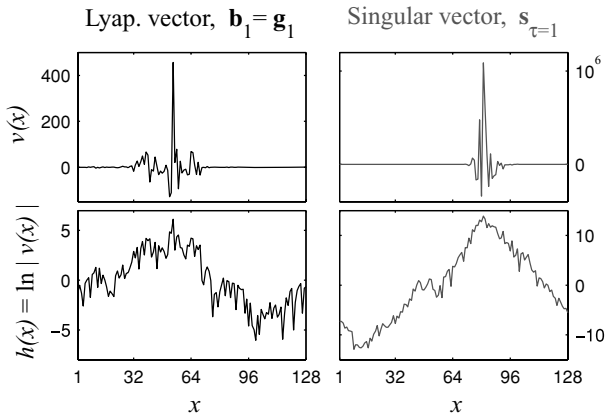

Fig. 3. First Lyapunov vector (left-hand panel), and singular vector for $\tau = 1$ (right-hand panel). Lower panels show their associated surfaces.

in which spatial correlations are progressively build up starting from an initially random, spatially uncorrelated perturbation. In this sense the error growth M alone is clearly insufficient to fully describe the problem.

To uncover the spatio-temporal structure of perturbations we propose here to make use of a successful approach to the problem that has been developed in the last few years and borrows concepts and tools from the close field of the statistical mechanics of surface growth in non-equilibrium extended systems. One decade ago a noticeable paper by Pikovsky and Politi (1998) (see also Pikovsky and Kurths, 1994) conjectured the existence of unexpected relation between perturbations in spatio-temporal chaos and scale-invariant surfaces in spatially extended stochastic systems. It is well known that the first LV ($\mathbf{b}_1 = \mathbf{g}_1$), exhibits dynamic localization (a typical snapshot for the L96 model is shown in Fig. 3) . Pikovsky and Politi (1998) noticed that a logarithmic (Hopf-Cole) transformation allows one to unfold the fine detail of the vector so its rich spatial structure can be better revealed. Nowadays, there is enough numerical evidence suggesting that, for a large family of spatially extended and homogeneous systems, this log-transformed LV exhibits correlations in space and time that are described by the canonical Kardar–Parisi–Zhang (KPZ) model for stochastic surface growth (Kardar et al., 1986):

$$\partial_t h = \xi + (\partial_x h)^2 + \partial_{xx} h, \tag{9}$$

where $\xi(x, t)$ is a (random) fluctuating term mimicking the short-ranged chaotic fluctuations. Roughly speaking, this surface picture arises from the fact that the growth of chaotic perturbations is generically multiplicative, which can be transformed into additive fluctuations by taking the logarithm.

The main advantage of studying the associated surface instead of the vector itself is that simple and powerful scaling laws emerge. It turns out that KPZ surfaces are scale-invariant fields and, therefore, nice scaling properties of the spatio-temporal correlations can be observed. Scale-invariant surfaces are statistically invariant under rescaling of the space coordinate, $x \to bx$, and time, $t \to b^{\alpha/\beta} t$, so that $h(x, t) \sim b^{-\alpha} h(bx, b^{\alpha/\beta} t)$, where the symbol $\sim$ means that the probability distribution is identical. This translates into a simple power-law form of the correlation function, $\langle \overline{|h(x, t) - h(x', t)|^2} \rangle = t^{2\beta} f(|x - x'|/t^{\beta/\alpha})$, where the exponents are robust (universal) to changes in the microscopic details of the system (Barabási and Stanley, 1995). The scaling function has the asymptotes $f(\rho) \sim \rho^{2\alpha}$ for $\rho \ll 1$, and $f(\rho) \sim$ const. for $\rho \gg 1$. Therefore, the growing correlation length $\ell(t) \sim t^{\beta/\alpha}$ plays a central role and determines the extent of spatial correlations that scale as

$$\langle \overline{|h(x, t) - h(x', t)|^2} \rangle \sim |x - x'|^{2\alpha}, \tag{10}$$

for two points at distance $|x - x'| \ll \ell(t)$. The 'roughness' exponent α and the growth exponent β characterize completely the scaling properties of the surface.

Inspired in this idea, we define the log-transformed vector $h(x, t) = \ln|v(x, t)|$, already introduced in the definition of M in eq. (8), as the 'surface' associated with the corresponding vector $\mathbf{v}(t)$. The present authors and co-workers have found that this transformation is also useful to study different types of perturbations. In several publications we have extended the theoretical framework of surface growth to finite random perturbations (López et al., 2004), bred vectors (Primo et al., 2005, 2006), Lyapunov vectors beyond the first one (Szendro et al., 2007; Pazó et al., 2008), and SVs (Pazó et al., 2009). The use of the surface $h(x, t) = \ln|v(x, t)|$ allows one to obtain many interesting scaling properties of the spatio-temporal correlations, which otherwise would be hidden in a strongly localized function $v(x, t)$. We refer to the interested reader to the recent literature on this problem.

In this paper we will exploit the scaling properties of the logarithm transform $h(x, t) = \ln|v(x, t)|$ to describe the spatial correlations. The insight provided by the associated surface is exemplified in Fig. 3. In the upper panels the 1st LV and the SV for $\tau = 1$ look similar. However, the associated surfaces shown in the bottom panels appear readily different even to the naked eye. For the LV, the surface has a random-walk-like shape, although the SV surface has a distorted triangular shape. This indicates that the SV is exponentially localized and its magnitude decays as $\sim \exp(-a\,|x - x_0|)$ from the localization center, while the LV instead presents a stretched-exponential spatial distribution $\sim \exp(-a\sqrt{|x - x_0|})$ around the current localization center x_0. The fine detail hidden in the spatial structure of any given vector considered in this paper can be immediately uncovered by studying the associated 'surface' that appears after the logarithmic transform.

Within the surface picture just described it is therefore crucial to consider the surface fluctuations. Therefore, in addition to the 'mean height' measured by M, Eq. (8), we have to calculate the

(squared) 'surface width'

$$V(t) = \left\langle \frac{1}{L} \sum_{x=1}^{L} [h(x,t) - M(t)]^2 \right\rangle, \tag{11}$$

which measures the time evolution of the fluctuations of the error growth around its mean value M. The surface width $V(t)$ for any initially random infinitesimal perturbation grows in time until it reaches a stationary value at long times. The time to reach the stationary state is known to increase as a power law with the system size.

$V(t)$ also gives an estimate of the localization strength–namely, how many magnitudes apart the peaks and the valleys of $v(x, t)$ are separated. Additionally, V serves to classify and characterize in a useful way all the vectors considered in this paper. It will be shown in the next section that the stationary (long-time) value of V for the first LV, V_1, can be used as a convenient reference point ($V_1 = 5.8$ in our L96 system of size $L = 128$) to compare with in order to give a quantitative measure of the degree of localization for each type of vector.

We also note that scale invariance (see eq. 10) immediately leads to the important formula

$$V(t) \sim \ell(t)^{2\alpha}, \tag{12}$$

$\ell(t)$ being the growing correlation length and α the so-called roughness exponent. Therefore, $V(t)$ can be used as an index that measures the extent of the spatial correlations, namely, the typical length scale over which the perturbation is uncorrelated, $\langle \overline{h(x,t)h(x',t)} \rangle - M^2(t) \to 0$ for $|x - x'| \gg \ell(t)$. For $1D$ surfaces in the KPZ universality class the exact result $\alpha = 1/2$ is well-known (Kardar et al., 1986; Pikovsky and Politi, 1998), so that $V(t) \sim \ell(t)$ is obtained.

6. Spatial structure and crossover length

Spatial correlations in extended systems, in particular for the associated surfaces introduced above, can be fully characterized by the power spectral density (PSD) or structure factor: $S(k) = \langle \hat{h}(k,t)\hat{h}(-k,t) \rangle$, where $\hat{h}(k,t) = L^{-1/2} \sum h(x,t) \exp(\imath k x)$ is the Fourier transform of the surface height $h(x, t)$. The PSD is usually computed in the long time limit where one expects to have $S(k) \sim k^{-(2\alpha+1)}$ with the roughness exponent α for a fully scale-invariant surface.

Figure 4 shows the PSDs for the several types of vectors discussed in this paper. We find that all types of vectors exhibit a clear separation of scales in the stationary state. Each vector surface is observed to exhibit a crossover wavenumber $k_\times$, which corresponds to a characteristic length scale $l_\times = 2\pi k_\times^{-1}$, such that $S(k) \sim k^{-2}$ for scales $k > k_\times$. All PSD coincide at scales below a certain scale $l_\times$. This means that bred, Lyapunov, and SVs are statistically indistinguishable when looked at these short-length scales, where the spatial correlations of any vector surface generically decay like $S(k) \sim k^{-2}$, as corresponds to KPZ behaviour ($\alpha = 1/2$). Also note that for very large k the PSD shows the expected deviation from the k^{-2} scaling, due to a lattice spacing effect on the discrete Fourier transform of the diffusion term as $k \to \pi/a$, where $a = 1$ is the lattice spacing (Barabási and Stanley, 1995).

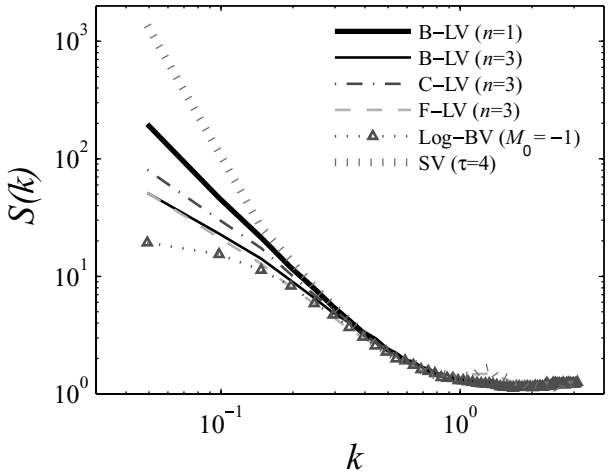

Fig. 4. Spatial power spectral densities of a representative set of vectors. For the SV only odd wavenumbers are used $k_m = 2\pi m/L (m$ odd); even wavenumbers are negligible due to the symmetry of the triangular structure. Each vector, with the exception of the first B-LV, exhibits a particular crossover wavenumber $k_\times$ where the PSD bends and departs from the 1st B-LV. A scaling law for $k < k_\times$ characterizes each vector type (see Table 2 for details).

On the other hand, the spatial structure of the perturbation at large-scales, $k < k_\times$, is indeed very interesting. It is important to note that a flat PSD indicates absence of correlation, while power-law decay of the PSD indicates long-range spatial correlation over the corresponding interval of k. One can immediately appreciate in Fig. 4 how the PSD for each particular vector exhibits different scaling behaviour (i.e. different degree of correlations) for wavenumbers $k < k_\times$. Table 2 summarizes the spatial properties of all the vector types. The scaling behaviour of correlations must be understood in the asymptotic limit of large system sizes. For instance, for the system sizes we used, the PSD of the Log-BV is still not completely flat ($\sim k^0$) at small k, but it does become asymptotically flat in the hydrodynamic limit for large enough systems, as it was shown by Primo et al. (2005, 2006).

The existence of the universal scaling relations in Table 2, reinforces the role of V as the variable that condenses very valuable information about the spatial structure and localization degree of any given vector. To be precise, according to Parseval's theorem V equals the area under the PSD curve, $V = \sum_{m=1}^{L/2} S(k_m)$. This immediately allows us to conclude that the SV is the most strongly localized vector (large V) among all the perturbation types, since its PSD has an area that exceeds all the others. Therefore, as discussed above, the surface width V gives a

Table 2. Spatial structure (crossover length and PSD) for the surfaces associated to different vector types (cf. Fig. 4)

Vector type	Cross. length $l_\times = \frac{2\pi}{k_\times}$	$S(k < k_\times)$	$S(k > k_\times)$	Reference
Log-BV	$\sim M_0^2$	Constant		Primo et al. (2005, 2006)
B-LV	$\approx (L/n)^\theta$ ($\theta \approx 1$)	k^{-1}		Szendro et al. (2007), Pazó et al. (2008)
F-LV	$\approx (L/n)^\theta$ ($\theta \approx 1$)	k^{-1}	k^{-2}	Pazó et al. (2009)
C-LV	$\approx (L/n)^\theta$ ($\theta \approx 1$)	$k^{-1.15}$		Szendro et al. (2007), Pazó et al. (2008)
SV	$\sim \tau^{\gamma/2}$ ($\gamma \simeq 0.78$)	k^{-4}		Pazó et al. (2009)

Notes: The scaling laws hold for large systems (see the references for details and supporting theoretical arguments).

compact and simple method to measure both the spatial correlation magnitude and the degree of localization, which can be used to compare different types of vectors.

7. MVL diagram

We now make use of the so-called MVL diagram (Primo et al., 2005, 2007; Gutiérrez et al., 2008) to analyse the evolution of perturbations. The MVL is constructed by plotting the evolution in time of the variance $V(t)$ versus perturbation size $M(t)$. The information so obtained allows a complete analysis and will be used in this paper as a tool to detect the distinct dynamics. The MVL diagram, for instance, has been recently used (Fenández et al., 2009) to successfully compare models in an ensemble prediction system and to provide information about how the corresponding ensemble had been initialized.

7.1. Stationary perturbations

Bred vectors (and Log-BVs) are usually generated as stationary perturbations that are periodically rescaled to a constant size. While a perturbation remains infinitesimal-like it stays approximately in the tangent manifold and the rescaling procedure does not affect the evolution of $V(t)$, which eventually converges to V_1. Recall that V_1 is the stationary value of the variance V for the main (truly infinitesimal) LV. However, if we allow the perturbation to go beyond a certain magnitude, the action of non-linear terms (López et al., 2004; Primo et al., 2005, 2006) kicks the perturbation out from tangent space, leading to the loss of correlation at long scales.

In order to visualize in the MVL diagram how these effects take place it is instructive to first plot the stationary $V(M_0)$ values of perturbations that are kept at a constant size M_0, which is the Log-BV for $\mathbf{l}_{M_0}$ by definition. In Fig. 5 one can see several curves, but let us by now focus on the black bold line. This line corresponds to the curve V versus M for stationary Log-BV perturbations that are periodically rescaled to have a 0-norm $\exp(M_0)$, according to the procedure discussed in Section 3.5. For small values of M_0 (say $M_0 < -8$) the perturbation dynamics is linear (approximatively stays within tangent space) and, thus, V is a M_0-independent constant $V(M_0) = V_1 \approx 5.8$; namely, the value corresponding to the first LV. In the interval of

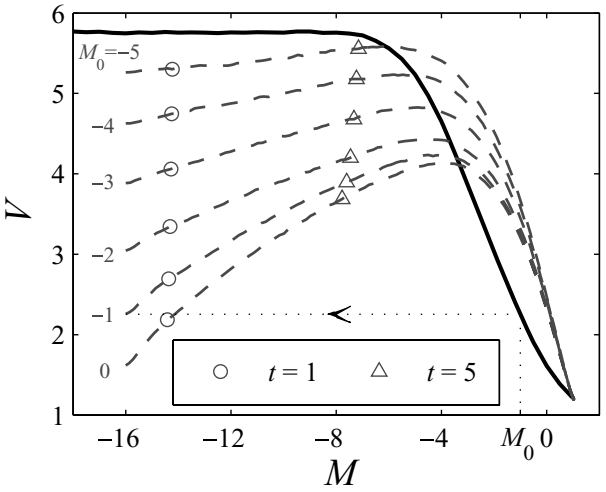

Fig. 5. Evolution in (M, V) coordinates of perturbations initialized by Log-BVs bred with different values of M_0. From top to bottom Log-BVs were generated setting $M_0 = -5, -4, \ldots, 0$. The initial perturbations were normalized to $M = -16$, and the circles (resp. the triangles) indicate the coordinates after $t = 1$ t.u. (resp. 5 t.u.). The trajectories have been averaged over 5000 realizations. The black bold line indicates the values of V for perturbations forced to stay at a given distance M_0 (log-bred vectors).

perturbation sizes $M_0 \in (-\infty, -8)$ the Log-BV is statistically indistinguishable from the first LV. When M_0 is set up above some threshold ($M_0 \approx -8$ in our simulations) non-linear effects destroy the correlations among distant parts of the vector. The spatial structure of the Log-BV in this regime follows the typical structure of the main LV, but only for scales below the crossover length $l_\times$ (as can be readily seen in Fig. 4).

The black bold line ends at $M_0 \approx 1$, $V(M_0 \approx 1) \approx 1.23$, where the perturbation becomes spatially uncorrelated and the corresponding surface exhibits Gaussian statistics. This point corresponds to the attractive fixed point for the free evolution of finite perturbations (Gutiérrez et al., 2008). The bold line in Fig. 5 will appear in subsequent figures because it serves as a good reference line indicating the regions corresponding to the linear/non-linear regime and localization strengths above/below the first LV. The line divides the phase space of perturbations into two parts. Well above the bold line perturbations are not adapted

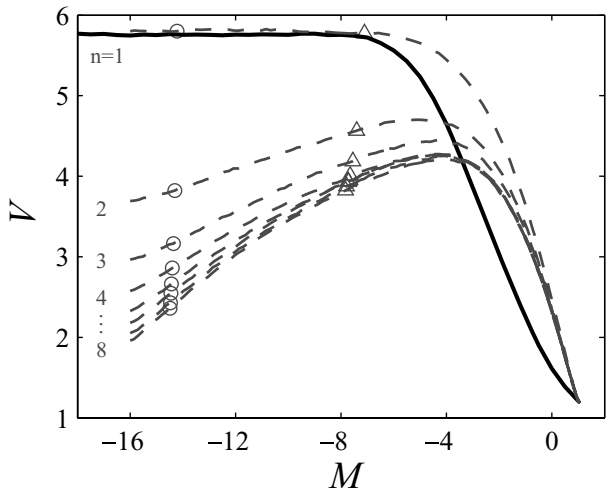

Fig. 6. Evolution of perturbations initialized by B-LVs, $n = 1, \ldots, 8$. For comparison we also plot (black bold line) the values of V for perturbations forced to stay at a given distance M_0 (log-bred vectors).

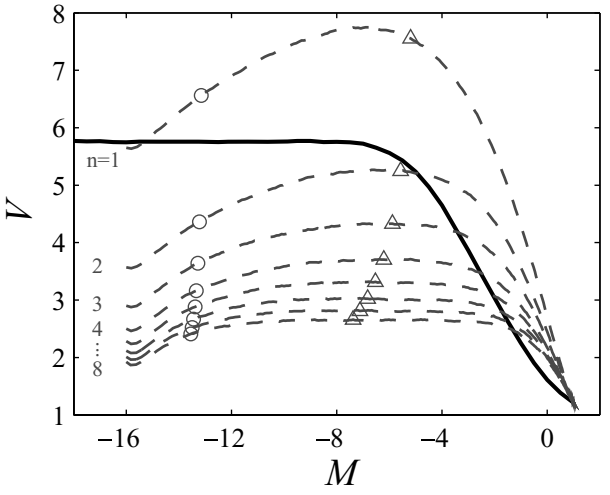

Fig. 7. Evolution of perturbations initialized by F-LVs, $n = 1, \ldots, 8$. For comparison we also plot (black bold line) the values of V for perturbations forced to stay at a given distance M_0 (log-bred vectors).

to the flow dynamics (i.e. point away from the attractor). We will refer to these perturbations as overlocalized.

The structure of the Log-BV has to be compared with the time evolution of 'bred perturbations' that are left to evolve freely after the breeding procedure. These curves are also shown in Fig. 5 but will be discussed in Section 8.

7.2. Interpretation of the MVL diagram

The MVL diagram can be seen as a kind of phase space of perturbations. Lines in the diagram can be complemented with symbols indicating the position of the perturbation in the MVL diagram after fixed temporal intervals. (see Figs. 5–9). When plotting the evolution of a finite perturbation in this manner we obtain a complete description of its dynamics.

(i) The perturbation size is exp $M(t)$, hence the abscissa of the diagram directly corresponds to the size in a logarithmic scale (see Section 4).

(ii) The variance $V(t)$ accounts for the spatial structure. It is a measure of the correlation of the corresponding surface $h(x, t)$ and can be also used as a localization strength index (see Section 5). Any finite perturbation becomes spatially uncorrelated and Gaussian distributed at long times ($t \gg t_s$). Therefore, one has the analytical asymptotics $V(t \gg t_s) = \pi^2/8 \approx 1.23$, which is independent of the initial perturbation and where the saturation time t_s scales with the system size. This clearly shows the robustness of V as a statistical indicator (see Section 7).

(iii) Once the corresponding perturbation (along a Log-BV, B-LV, F,LV, C-LV or SV) is left to evolve freely, the slope of the $V(t)$ versus $M(t)$ curve provides information about its dynamic adaptation. A positive slope indicates a progressive increase of

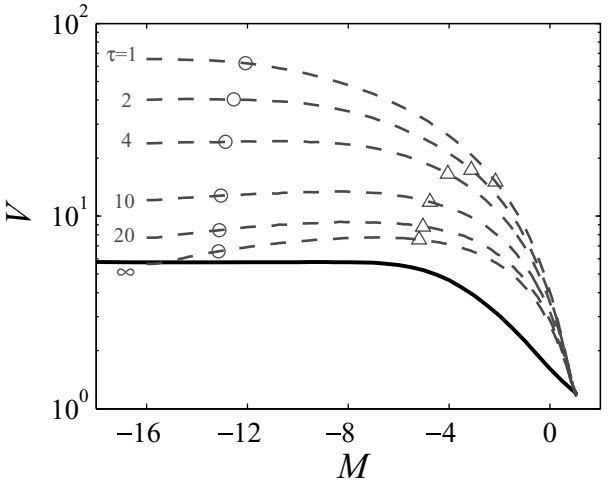

Fig. 8. Evolution of perturbations initialized by SVs for different values of the optimization time τ. Due to the strong (exponential) localization of these vectors we have put the y-axis in logscale. For comparison we also plot (black bold line) the values of V for perturbations forced to stay at a given distance M_0 (log-bred vectors).

spatial correlation, which usually appears when perturbations are in the attractor and converging to the main Lyapunov vector. On the contrary, negative slopes mean that the perturbation is badly adapted and correlations must be rebuilt to reach the attractor (see e.g. Primo et al., 2007). A zero slope, $V(t) \sim$ const., means a stable structure—namely, a perfect dynamic embedding into the attractor. In this case the growth of $M(t)$ is always proportional to time.

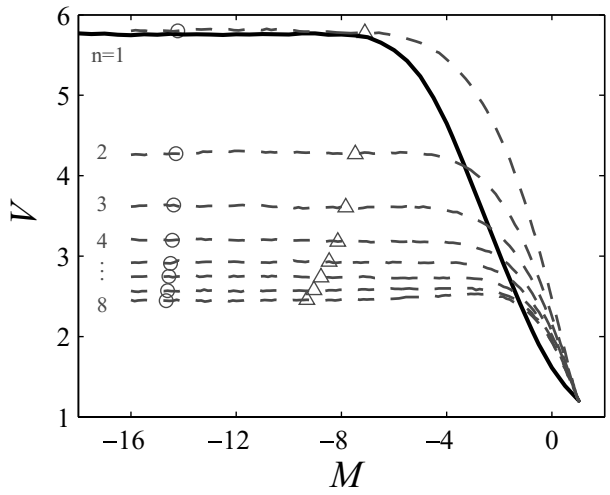

Fig. 9. Evolution of perturbations initialized by C-LVs, $n = 1, \ldots, 8$. For comparison we also plot (black bold line) the values of V for perturbations forced to stay at a given distance M_0 (log-bred vectors).

8. Free evolution of finite perturbations

The free evolution of a given finite perturbation obviously depends on how the specific perturbation we are looking at has been generated. Generally, vectors generated within the chaotic attractor continue their evolution in the attractor when left to evolve freely, until they become too large and non-linear effects come into play. In contrast, vectors that are dynamically not well adapted evolve towards the attractor after a transient period of dynamic adaptation. As discussed in the previous section, the MVL diagram is a very appropriate tool to detect these distinctly different behaviours with a minimal computational cost.

Using the same procedure described in Section 4 to obtain Fig. 2, the following numerical study is now carried out: (i) The initial perturbation is proportional to one of the particular vector types, $\mathbf{v}(t=0) \propto \{\mathbf{b}_n, \mathbf{f}_n, \mathbf{g}_n, \mathbf{s}_\tau, \mathbf{l}_{M_0}\}$, which have been constructed following the definitions given in Section 3. In doing so, we are certain that the initial perturbation $\mathbf{v}(t=0)$ has developed the corresponding spatial correlations. (ii) All initial perturbation types are then rescaled at present time $t = 0$ to a common size $M(t=0) = -16$, so that we are certain of being well inside the linear regime. (iii) Finally, the perturbed trajectory is left to evolve freely. The evolution of the perturbation (i.e. the difference between perturbed and control systems) is tracked on an MVL diagram. Note that the value of the variance $V(t=0)$ is intrinsic for each vector type; i.e. it does not depend on the rescaling applied, because multiplication by a factor only changes the amplitude (size) of the vector but has no effect on the spatial correlations.

Figures 5–9 show the evolution of the free perturbations for the different types of vectors considered in this paper. The behaviour observed varies drastically depending on the specific vector used for the initial perturbation, which indicates, at a first sight, that a certain control on a potential ensemble is feasible. As important characteristics to be controlled we focus on the growth rate, the localization strength, and the stability of the spatial structure.

The computation interval (see Table 1) used to initialize each perturbation vector plays a crucial role in the future dynamics of the free perturbation. It turns out that it defines the information content that the vector has about either the past or future dynamics. In what follows we use it as the most distinctive characteristics.

8.1. *Vectors generated from the past* $[-\infty, 0]$*: dynamic scaling*

Perturbations initialized along vectors generated only from the past, Log-BVs (Fig. 5) and B-LVs (Fig. 6), exhibit similar behaviour. We saw in Fig. 2 that they share the growth rate $\simeq \lambda_1$. In addition, if M_0 (for the Log-BV), and n (for the B-LV) are selected so that their typical localization lengths are the same (i.e. $V(t=0)$ coincides), their trajectories on the MVL diagram almost overlap. Hence, we arrive to the not-so-intuitive conclusion that perturbations initialized by Log-BVs and B-LVs, although generated in different ways, capture roughly the same degrees of freedom. They are well adapted perturbations that tend to converge to the main LV when they are let to evolve freely. Since they are well adapted perturbations at present time $t = 0$ one observes no transient period out of the attractor for $t > 0$. Then the MVL diagram shows a typical curve whose convexity (functional form $V \sim M^{2/3}$, Primo et al., 2008) is a consequence of the dynamic scaling ($V \sim t^{2\beta}$, with $\beta = 1/3$) characteristic of the universal growth of KPZ surfaces (Kardar et al., 1986; Barabási and Stanley, 1995). Hence the spatial structure is not stable but changes slowly, as a power law of time.

8.2. *Vectors adapted to the far future* $[0, \infty]$*: transient dominated evolution*

When the finite perturbation is initialized with vectors generated using the future trajectory of the system, i.e. F-LVs, there exists the possibility of varying the growth rates below λ_1. However, with information only about the future, these vectors are not well adapted dynamically and this is made apparent in the MVL diagram (see Fig. 7).

For finite perturbations initialized with F-LVs (see Fig. 7), the evolution of $V(t)$ exhibits an initial negative slope, which indicates a loss of spatial correlation and bad adaptation, followed by a severe transient that even becomes overlocalized [$V(t)$ overcoming the black bold line] for the perturbation corresponding to the first F-LV. The nth F-LV is expected to asymptotically converge to the nth C-LV, but convergence is extremely slow. Perturbed initial states using the nth F-LV evolve as finite perturbations and this convergence is hampered by non-linear effects,

which appear very early impeding this observation. The spatial structure of this type of perturbation strongly changes, already in the regime of (quasi-)infinitesimal evolution. As shown in Fig. 2, this produces a transient in the evolution of $M(t)$, and the long-term growth rate λ_n cannot be observed. The whole evolution of the finite perturbation is dominated by the transient.

8.3. *Vectors generated in finite-time intervals: maintained overlocalization*

The evolution of finite perturbations initialized with SVs is shown in the MVL diagram of Fig. 8. We can observe the fastest growth among all vectors with an apparent stable structure. This stability is only a transient since the spatial structure does not have much time to change due to the very fast growth. As a consequence the overlocalized initial structure is maintained along the evolution until the action of non-linear effects that appear when the perturbation has grown too large. Note that a similar behaviour should be expected for any other dynamic vector generated over finite-time intervals. As we explained in (Pazó et al., 2009), there exist universal laws connecting the overlocalized structure and the interval of the optimization time τ.

8.4. *Vectors adapted to the whole past/future trajectory: structural stability*

Characteristic Lyapunov vectors are computed using both the past and the future evolution of the control trajectory and, therefore, are the only vectors that have the possibility of a complete control of the growth rates. The corresponding Lyapunov exponents show up immediately $M(t) \sim \lambda_n t$ (Fig. 2). Interestingly, due to the intrinsic covariant character of C-LVs [see Eq. (4)], finite perturbations initialized with C-LV are also covariant within the linear regime. This is clearly seen in Fig. 9, where one can see that the variance V stays constant within the linear regime.

The robustness in the quasi-infinitesimal regime of a finite perturbation initialized with a characteristic vector is indeed remarkable. C-LVs are covariant with the linearized dynamics, and computational errors and non-linearities produce only a marginal instability. In Fig. 10 , we show that the structure of a perturbation initialized along a C-LV ($n = 3$) does not collapse to the main LV after being rescaled eight times!

9. Preparing initial ensembles

Differences between members of an ensemble have to be treated in the context of finite perturbations. In real forecasting the initial ensemble is calibrated to yield a reliable set of members able to represent a probabilistic functional space with some desired property. Four different properties are much sought after when preparing ensembles (Sections 9.1–9.4).

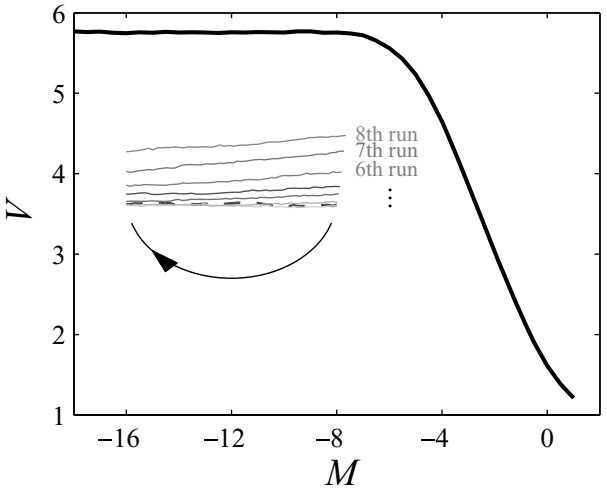

Fig. 10. Evolution of a perturbation initialized by the 3-rd C-LV and $M(t = 0) = -16$. Every 5 t.u. the perturbation has been normalized to $M = -16$. The spatial structure, measured by V, departs very slowly from its initial value, indicating the structural robustness of the C-LV. For comparison we also plot (black bold line) the values of V for perturbations forced to stay at a given distance M_0 (log-bred vectors).

9.1. *Dynamic adaptation*

An ensemble initialized with random perturbations is obviously the easiest choice, but also the least convenient. Vectors used in this paper have the advantage of including information about the dynamics of the system. However, only vectors that contain information from the past are well adapted to the attractor. One can view the chaotic attractor as a structure built from the remote past by the stretching-and-folding mechanism. A perturbation that has evolved within the flow will capture the attractor structure. Vectors using only information about the future (F-LVs and SVs) cannot be expected to reflect the geometry of the attractor. When adaptation to the trajectory is limited to a finite time, as in the case of SVs, the perturbation is not well immersed into the flow dynamics and becomes (somewhat artificially) overlocalized.

9.2. *Reliability and equivalence among members of an ensemble*

Members of an ensemble should be equivalent to each other in order to forecast with uniform probability (Kalnay, 2002). The best way to produce equivalent members in the ensemble is to use exactly the same generating procedure for all of them. However, at the same time the ensemble should have enough diversity to avoid the collapse of all members of the ensemble to the same vector.

Among the different vectors studied in the preceding sections, only Log-BVs provide initial perturbations such that each vector is uncorrelated at long scales. This translates into a flat spectrum

at long scales: $S(k) \sim$ const. for $k < 2\pi l_{\times}^{-1}$. This implies that one could construct an ensemble of Log-BVs, each member bred for a sufficiently long time with a different value of M_0 from random initial perturbations. The control parameter M_0 controls the typical extent of spatial correlations, $l_{\times}$, (see Table 2), and this determines the maximal number of statistically uncorrelated vectors, which should be approximately $L/l_{\times}$. Moreover, Log-BVs are true finite fluctuations generated by the actual model without the need of obtaining the tangent space equations, which in the case of operative weather models reduces considerably the degree of complication. Hence, in order to obtain dynamically adaptation and reliable ensembles Log-BVs offer a very simple an convenient option.

Vectors, other than Log-BVs, are not equivalent, and the ensemble's members must hence be built as linear combinations of vectors. The study of methods to produce reliable and controlled members from combination of Lyapunov vectors goes beyond our aim in this paper. However, we would like to underline the great utility that the characterization of finite perturbations from their spatial structure provides. Coefficients of the linear combination could be determined with the condition of producing a given structure.

9.3. The analysis error

Another possible strategy is to prepare an ensemble capable of capturing differences between the analysis and the true atmospheric state (the so-called 'analysis error'). This property had initially been sought after in the context of bred vectors. In fact, bred vectors were postulated as initial conditions of ensembles due to their similarity to the 'error of the day'(analysis error for a day) (Kalnay, 2002). To achieve this goal one calibrates the statistics generated by the flow dynamics with that of the analysis error. Dynamically adapted vectors from the past (Log-BVs, B-LVs and C-LVs) are then good candidates to generate the desired ensemble.

9.4. The fastest spread

Another strategy of ensemble construction is to consider the members of the ensemble spreading with the fastest growth rate to capture the amplified errors in a given time. This is the property initially used in the European Center (ECMWF) to prepare ensembles (Molteni et al., 1996). By definition SVs are the optimal choice in this case. Note however that this is not compatible with other desired properties discussed in Sections 9.1–9.3. Perturbations with growth rates greater than λ_1 immediately imply that those are independent of the flow dynamics. SVs are then overlocalized perturbations. In systems with strong chaos SVs would be unrealistic perturbations that should be prepared before being used as initial perturbations. In weather models this is accomplished, for instance, with the so called rotated SVs (Molteni et al., 1996).

9.5. The optimal ensemble: why should we be using covariant dynamic modes (C-LVs)?

Regarding preparation of ensembles for initial perturbations characteristic Lyapunov vectors, among all vectors studied in this work, clearly appear to be the most convenient in almost all respects: (i) they are independent of the scalar product used and, therefore, they are not norm dependent; (ii) they are well adapted to the flow dynamics (capturing spatial locations where the perturbation is growing) and also containing information about the future (highlighting the locations that are going to grow); (iii) they allow a control of the growth rate (below λ_1) and (iv) finite perturbations initialized by C-LVs are structurally stable (maintaining the spatial correlations) and become affected by non-linear effects only marginally. Practically they can be used as intrinsic dynamic modes of the system at hand. Then, why not use them in ensemble prediction systems? A major concern to bear in mind is that C-LVs are probably the most expensive to obtain from a computational point of view. However, the possibilities they offer of control and their remarkable structural stability are overwhelming and may be strong enough arguments to be seriously considered in real forecasting. Further research in this direction with realistic weather models would be extremely interesting.

10. Conclusions

A thorough and comparative study of the potential use of bred, singular, and Lyapunov vectors in a probabilistic forecasting method based on ensembles has been carried out. We have used the simple Lorenz '96 model to obtain numerical comparison among perturbations initialized by different types of vectors.

General considerations to achieve a certain control in the ensemble evolution have been discussed along the paper. Besides the classical analysis of the exponential growth rate we have also included a novel analysis of the spatial structure. Spatial structure of perturbations, i.e. the form of the spatial correlations, has been neglected in previous studies in the field, mostly due to the lack of proper tools for the analysis. We have shown that the study of the logarithmic transform of the perturbation allows us to disentangle the puzzle of the spatial organization of perturbations.

The MVL diagram together with the spectral density analysis offer powerful tools to uncover the dynamics not only of the error growth but also the evolution of the spatial correlations, which are the main distinctive features of perturbations in extended systems. We have shown that both are related trough universal scaling laws that arise from the dynamic scaling observed in the logarithmic transformation (the vector surfaces). Scaling laws are generic properties in chaotic extended systems and provide useful tools to determine the limits on the control of the evolution of the ensemble. We have not entered in detail in the origin of

these scaling laws in this paper but referred to the interested reader to the recent and abundant publications dealing with this issue.

We have seen in our study that some vector types point off the attractor whereas others are more or less tangent to it. Vectors can be affected by strong transients or not; they can even be stationary (C-LVs). Each vector type has distinctive properties stemming from the time interval used in its generation (past versus future, finite versus infinite) and from the method itself (breeding, orthogonalization, optimization). These properties provide each vector with particular features for the generation of initial ensembles or for their evolution:

(i) Correlation and diversity of ensembles. Log-BVs (for large enough M_0) provide perturbations that are completely uncorrelated at long scales, which means such a high degree of diversity that they can be used directly as members of the ensemble. In contrast, B-LVs, F-LVs and C-LVs exhibit spatial correlations [albeit small, $S(k) \sim 1/k$] even at the largest scales. A similar degree of diversity could be possibly achieved in this cases but only after a proper linear combination of vectors (not discussed here). In the case of perturbations initialized with SVs, we found they lead to strongly correlated (localized) perturbations at large-scales, which immediately implies a low degree of diversity and the need of additional methods to construct a proper and diverse ensemble.

(ii) Growth rate. Control of the exponential growth rate is only possible with the use of Lyapunov vectors involving backward integration from the future. On the contrary, B-LVs and bred vectors, having only information from the past, behave in good approximation as free evolving fluctuations with an exponential growth rate close to the first Lyapunov exponent. Slow growth, with an exponential rate less than the first Lyapunov exponent, is obtained from F-LVs and C-LVs, but only C-LVs keep a stable structure that guarantees a constant growth rate. Fast amplification, with exponential growth rates greater than the first Lyapunov exponent is obtained from SVs. However, their spatial structure is overlocalized, which implies the use of perturbations pointing off the flow.

(iii) Spatial structure. The spatial structure is stable only in the case of C-LVs. When the other vectors are used as initial perturbations we found that they tend either to the main LV (Log-BVs, B-LVs) or to their corresponding C-LV (F-SVs). Also SVs tend to the main LV, but with a very slow convergence.

To conclude, initial perturbations initialized with C-LVs offer the best performance allowing a precise control of the growth rate and a robust structural stability. They are computationally expensive, but the many advantages they exhibit may well compensate the numerical costs. Further research with operative weather models in this direction would be certainly worth the effort given the potential impact in forecasting methods that the use of C-LVs could bring about.

11. Acknowledgments

DP acknowledges the support by CSIC under the Junta de Ampliación de Estudios Programme (JAE-Doc). Financial support from the Ministerio de Educación y Ciencia (Spain) under projects FIS2006-12253-C06-04 and CGL2007-64387/CLI is acknowledged.

References

Barabási, A.-L. and Stanley, H. E. 1995. *Fractal Concepts in Surface Growth*, Cambridge University Press, Cambridge.

Benettin, G., Galgani, L., Giorgilli, A. and Strelcyn, J.-M. 1980. Lyapunov characteristic exponents for smooth dynamical systems and for Hamiltonian systems. *Meccanica* **15**, 9.

Eckmann, J.-P. and Ruelle, D. 1985. Ergodic theory of chaos. *Rev. Mod. Phys.* **57**, 617–656.

Errico, R. M. and Langland, R. 1999. Notes on the appropriateness of "bred modes" for generating initial perturbations used in ensemble prediction. *Tellus* **51A**(3), 431–441. doi:10.1034/j.1600-0870.1999.t01-3-00007.x.

Ershov, S. V. and Potapov, A. B. 1998. On the concept of stationary Lyapunov basis. *Physica D* **118**(3-4), 167–198. doi:10.1016/S0167-2789(98)00013-X.

Fenández, J., Primo, C., Cofiño, A., Gutiérrez, J. M. and Rodríguez, M. A. 2009. MVL spatiotemporal analysis for model intercomparison in EPS: application to the DEMETER multi-model ensemble. *Clim. Dyn.* **33**, 233–243. doi:10.1007/s00382-008-0456-9.

Gutiérrez, J. M., Primo, C., Rodríguez, M. A. and Fernández, J. 2008. Spatiotemporal characterization of ensemble prediction systems: the mean-variance of logarithms (MVL) diagram. *Nonlin. Processes Geophys.* **15**(1), 109–114. **URL**: http://www.nonlin-processes-geophys.net/15/109/2008/

Kalnay, E. 2002. *Atmospheric Modeling, Data Assimilation and Predictability*, E. Cambridge University Press, Cambridge.

Kardar, M., Parisi, G. and Zhang, Y.-C. 1986. Dynamic scaling of growing interfaces. *Phys. Rev. Lett.* **56**(9), 889–892. doi:10.1103/PhysRevLett.56.889.

Legras, B. and Vautard, R. 1996. A guide to Liapunov vectors. In: *Proceedings of the Seminar on Predictability* Vol. I, (ed. T. Palmer). ECWF Seminar, ECMWF, Reading, UK, pp. 135–146.

López, J. M., Primo, C., Rodríguez, M. A. and Szendro, I. G. 2004. Scaling properties of growing noninfinitesimal perturbations in space–time chaos. *Phys. Rev. E* **70**(5), 056224. doi:10.1103/PhysRevE.70.056224.

Lorenz, E. N. 1996. Predictability a problem partly solved. In: *Proceedings of the Seminar on Predictability* Vol. I, (ed. T. Palmer), ECWF Seminar, ECMWF, Reading, UK, pp. 1–18.

Lorenz, E. N. and Emanuel, K. A. 1998. Optimal sites for supplementary weather observations: simulations with a small model. *J. Atmos. Sci.* **55**(3), 399–414. doi:10.1175/1520-0469(1998)055<0399:OSFSWO>2.0.CO;2.

Molteni, F., Buizza, R., Palmer, T. N. and Petroliagis, T. 1996. The ECMWF ensemble prediction system: Methodology and validation. *Quart. J. Roy. Meteor. Soc.* **122**, 73–119.

Pazó, D., Szendro, I. G., López, J. M. and Rodríguez, M. A. 2008. Structure of characteristic Lyapunov vectors in spatiotemporal chaos. *Phys. Rev. E* **78**(1), 016209. doi:10.1103/PhysRevE.78.016209. **URL**: http://link.aps.org/abstract/PRE/v78/e016209

Pazó, D., López, J. M. and Rodríguez, M. A. 2009. Exponential localization of singular vectors in spatiotemporal chaos. *Phys. Rev. E* **79**(3), 036202. doi:10.1103/PhysRevE.79.036202. **URL**: http://link.aps.org/abstract/PRE/v79/e036202

Pikovsky, A. and Politi, A. 1998. Dynamic localization of Lyapunov vectors in spacetime chaos. *Nonlinearity* **11**(4), 1049–1062. doi:10.1088/0951-7715/11/4/016.

Pikovsky, A. S. and Kurths, J. 1994. Roughening interfaces in the dynamics of perturbations of spatiotemporal chaos. *Phys. Rev. E* **49**(1), 898–901. doi:10.1103/PhysRevE.49.898.

Primo, C., Rodríguez, M. A., López, J. M. and Szendro, I. 2005. Predictability, bred vectors, and generation of ensembles in space–time chaotic systems. *Phys. Rev. E* **72**(1), 015201. doi:10.1103/PhysRevE.72.015201.

Primo, C., Szendro, I. G., Rodríguez, M. A. and López, J. M. 2006. Dynamic scaling of bred vectors in spatially extended chaotic systems. *Europhys. Lett.* **76**, 767. doi:10.1209/epl/i2006-10370-7.

Primo, C., Szendro, I. G., Rodríguez, M. A. and Gutiérrez, J. M. 2007. Error growth patterns in systems with spatial chaos: from coupled map lattices to global weather models. *Phys. Rev. Lett.* **98**(10), 108501. doi:10.1103/PhysRevLett.98.108501. **URL**: http://link.aps.org/abstract/PRL/v98/e108501

Primo, C., Rodríguez, M. A. and Gutiérrez, J. M. 2008. Logarithmic bred vectors. A new ensemble method with adjustable spread and calibration time. *J. Geophys. Res.* **113**. D05116.

Ruelle, D. 1979. Ergodic theory of differentiable dynamical systems. *Phys. Math. IHES* **50**, 27–58.

Smith, L. A. 2001. Disentangling uncertainty and error: On the predictability of nonlinear systems. In: *Nonlinear Dynamics and Statistics* (ed. A. I. Mees), Birkhäuser Verlag, Boston.

Szendro, I. G., Pazó, D., Rodríguez, M. A. and López, J. M. 2007. Spatiotemporal structure of Lyapunov vectors in chaotic coupled-map lattices. *Phys. Rev. E* **76**(2), 025202. doi:10.1103/PhysRevE.76.025202. **URL**: http://link.aps.org/abstract/PRE/v76/e025202

Toth, Z., Szunyogh, I., Kalnay, E. and Iyengar, G. 1999. Comments on: "Notes on the appropriateness of 'bred modes' for generating initial perturbations". *Tellus* **51A**(3), 442–449. doi:10.1034/j.1600-0870.1999.t01-3-00008.x.

Tracton, M. S. and Kalnay, E. 1993. Operational ensemble prediction at the national meteorological center: practical aspects. *Wea. Forecast.* **8**, 379–398.

Wei, M. and Frederiksen, J. S. 2004. Error growth and dynamical vectors during Southern Hemisphere blocking. *Nonlin. Processes Geophys.* **11**(1), 99–118. **URL**: http://www.nonlin-processes-geophys.net/11/99/2004/

Wolfe, C. L. and Samelson, R. S. 2007. An efficient method for recovering Lyapunov vectors from singular vectors. *Tellus* **59A**(3), 355–366. doi:10.1111/j.1600-0870.2007.00234.x.